NASA Technical Memorandum 87200

A Numerical Simulation of the Inviscid Flow Through A Counter-Rotating Propeller

Mark L. Celestina, Richard A. Mulac
Sverdrup Technology, Inc.
Lewis Research Center
Cleveland, Ohio

and

John J. Adamczyk
Lewis Research Center
Cleveland, Ohio

Prepared for the
31st International Gas Turbine Conference
sponsored by the American Society of Mechanical Engineers
Dusseldorf, West Germany, June 8–12, 1986

NASA

A NUMERICAL SIMULATION OF THE INVISCID FLOW THROUGH A COUNTER-ROTATING PROPELLER

Mark L. Celestina and Richard A. Mulac
Sverdrup Technology, Inc.
Lewis Research Center
Cleveland, Ohio 44135

and

John J. Adamczyk
National Aeronautics and Space Administration
Lewis Research Center
Cleveland, Ohio 44135

E-2855

SUMMARY

This paper presents the results of a numerical simulation of the time-averaged inviscid flow field through the blade rows of a multiblade row turboprop configuration. The governing equations are outlined along with a discussion of the solution procedure and coding strategy. Numerical results obtained from a simulation of the flow field through a modern high-speed turboprop will be shown.

INTRODUCTION

Solving the flow field of a multiblade row machine is very difficult considering the time and length scales involved. The numerical simulation of a general configuration remains formidable even for a machine much larger and faster than today's Class VI computers. However, by mathematically modeling the flow field in the spirit of Reynolds-averaged modeling of turbulent flows, much of the physics relevant to design can be deduced (ref. 1). The objective of this paper is to describe a procedure for simulating the inviscid, time-average flow through a multiblade row geometry and present results for a counter-rotating propeller configuration designed to operate at transonic speeds.

Three-dimensional, inviscid codes have been developed for isolated propellers using a variety of algorithms. Bober, et al. (ref. 2) and Barton, et al. (ref. 3) used the Beam and Warming algorithm and obtained good comparisons to experimental results. Clark (ref. 4) used Denton's finite volume code modified for propellers to obtain solutions for acoustical analyses. Holmes and Tong (ref. 5) applied Jameson's Runge-Kutta procedure (ref. 6) formulated in terms of cartesian velocity components to a turbine, compressor, and propeller blade row. Celestina and Adamczyk (ref. 7) presented results applying Jameson's technique formulated in terms of cylindrical velocity components to a turbine and propeller blade row.

A procedure for extending isolated blade row analyses to multiblade row configurations was suggested by Denton (ref. 8). His method as applied to a stage involved circumferentially averaging the flow properties at a given axial location between the two blade rows. By doing so, the downstream boundary

condition to the first blade row and upstream boundary condition to the second blade row are circumferentially uniform.

Adamczyk (ref. 1) developed a first principles procedure for analyzing multiblade row flows in which a sequence of averaging operators are used to derive a set of equations that describes an "averaged" three-dimensional representation of the flow field through each blade row of a multiblade row machine. This flow field is steady in time in a reference frame fixed to each blade row and spatially periodic from passage to passage. The field equations associated with this model are referred to as the average-passage equation system. The present work is therefore unique in that it outlines a procedure to solve a set of equations which govern a three-dimensional multiblade row flow field that is directly traceable to the Navier-Stokes equations. However, this average-passage description has associated with it a well known difficulty. Averaged equations of motion always lead to situations in which there are more unknowns than equations - this is the "closure" problem which requires assumptions or empirical information to make the number of equations equal to the number of unknowns. The closure problem is addressed for the inviscid form of the equations by Adamczyk in reference 9.

The procedure for solving the average-passage equation system requires a mesh for each blade row. The axial and radial location of each grid point is identical for each mesh, but varies in the circumferential direction due to relative blade row locations and unequal blade numbers. A solution is generated for each blade row on its own mesh with the effect of the neighboring blade row contained in source terms in the governing equations. The source terms are sequentially updated using information provided by the neighboring blade row simulation.

GOVERNING EQUATIONS

The three-dimensional average-passage equation system for simulating the flow through multiblade rows can be written in cylindrical (r,θ,z) coordinates as

$$(\lambda \underline{u})_t + L(\lambda \underline{u}) + \int \lambda \underline{S}\, dVol = \int \lambda \underline{K}\, dVol \qquad (1)$$

The vector $\underline{u}$ contains the flow variables density, axial and radial momenta, angular momentum and total internal energy and λ is the neighboring blade row blockage factor. The value of this parameter ranges between zero and unity, unity being the value associated with zero blade thickness. (See ref. 1 for details.) The operator $L(\lambda \underline{u})$ balances the mass, axial and radial momenta, angular momentum, and energy through a control volume, $\int \lambda \underline{K}\, dVol$ is a source term due to the cylindrical coordinate system, and $\int \underline{S}\, dVol$ contains the body forces, energy sources, momentum, and energy temporal mixing correlations associated with the neighboring blade row(s). The details for computing these terms are given in a companion paper (ref. 9). The vector $\underline{u}$ and the operator $L(\lambda \underline{u})$ are defined by the following expressions:

$$u = [\rho, \rho v_r, r\rho v_\theta, \rho v_z, \rho e_o]$$

$$L(\lambda \underline{u}) = \int_{dA} [\lambda \underline{F} \cdot d\underline{A}_r + \lambda \underline{G} \cdot d\underline{A}_\theta + \lambda \underline{H} \cdot d\underline{A}_z] \tag{2}$$

where

$$\underline{F}^T = \left[\rho v_r, \rho v_r^2 + p, r\rho v_\theta v_r, \rho v_z v_r, \rho H v_r\right]$$

$$\underline{G}^T = \left[\rho v_\theta, \rho v_r v_\theta, r\left(\rho v_\theta^2 + p\right), \rho v_z v_\theta, \rho H v_\theta\right]$$

$$\underline{H}^T = \left[\rho v_z, \rho v_r v_z, r\rho v_\theta v_z, \rho v_z^2 + p, \rho H v_z\right]$$

$$\underline{K}^T = \left[0, \frac{\rho v_\theta^2 + p}{r}, 0, 0, 0\right]$$

In the above equations ρ represents the density, v_r, v_θ, and v_z are the radial, tangential, and axial absolute velocities and p is the pressure. From the equation of state the total internal energy is related to the pressure as follows

$$e_o = \frac{p}{\rho(\gamma - 1)} + \frac{1}{2}\left(v_r^2 + v_\theta^2 + v_z^2\right)$$

and the total enthalpy is related to e_o, p and by the equation

$$H = e_o + \frac{p}{\rho}$$

In the above equations all lengths are nondimensionalized by the diameter of the largest blade row. The velocity components are nondimensionalized by the reference speed of sound, $a_{ref}/\sqrt{\gamma}$, pressure and density by their respective reference values, and γ is the ratio of specific heats.

For rotating flows, the absolute (fixed) reference frame is transformed to the relative (rotating) frame by the transformation

$$\theta_{absolute} = \theta_{relative} + \Omega t \tag{3}$$

where Ω is the rotational wheel speed (positive with θ). Introducing equation (3) into equation (1) yields

$$L(\lambda \underline{u}) = \int_{dA} \lambda \underline{F} \cdot d\underline{A}_r + \lambda(\underline{G} - r\Omega \underline{u}) \cdot d\underline{A}_\theta + \lambda \underline{H} \cdot d\underline{A}_z \tag{4}$$

The term $(\underline{G} - r\Omega\underline{u}) \cdot d\underline{A}_\theta$ represents the relative flux of $\underline{u}$ in the tangential direction.

Equation (1) is discretized in space for a cell volume (fig. 1) by approximating the surface integrals by the mid point rule. The result is a system of ordinary differential equations of the form

$$\frac{d}{dt}(\lambda \underline{u}) + \sum \left[\lambda \underline{F}\, d\underline{A}_r + \lambda(G - r\Omega \underline{u})\, d\underline{A}_\theta + \lambda \underline{H} d\underline{A}_z \right] + \int \lambda \underline{S}\, dVol = \int \lambda K d\, Vol \quad (5)$$

The surface areas, $d\underline{A}_r, d\underline{A}_\theta, d\underline{A}_z$ are calculated using the cross product of the diagonals of a cell face and the volume is determined using the formula described by Holmes and Tong (ref. 5). Since all the flow quantities are cell-centered, a simple averaging procedure is used to determine the value of a variable at any surface, excluding solid boundaries. This is equivalent to second-order accurate central differencing for a uniform mesh.

Runge-Kutta Integration

To advance the equations in time, a four-stage Runge-Kutta scheme is used. The scheme employed has been patterned after the work of Jameson, et al. (ref. 6). Given information at time level n, the steps to advance to the next level, n + 1, are

$$\left.\begin{aligned} \underline{u}^{\alpha} &= \underline{u}^{n} - \alpha\, \Delta t L(\underline{u}^{n}) \\ \underline{u}^{\beta} &= \underline{u}^{n} - \beta\, \Delta t L(\underline{u}^{\alpha}) \\ \underline{u}^{\gamma} &= \underline{u}^{n} - \gamma\, \Delta t L(\underline{u}^{\beta}) \\ \underline{u}^{*} &= \underline{u}^{n} - \Delta t L(\underline{u}^{\gamma}) \\ \underline{u}^{n+1} &= \underline{u}^{*} + D(u^{*}) \end{aligned}\right\} \quad (6)$$

where $\alpha = 1/4$, $\beta = 1/3$, $\gamma = 1/2$ and $D(\underline{u})$ is the dissipation operator. The maximum permissible time step for this scheme is restricted by the CFL stability limit. Jameson has determined the limit for the above four-stage scheme to be $2\sqrt{2}$ based on a one-dimensional model problem. To enhance the convergence rate of this scheme, a local time step is chosen based on the maximum CFL number commensurate with stability. An advantage of using the present Runge-Kutta scheme is that it minimizes storage requirements.

Artificial Dissipation

To suppress odd-even point decoupling in the solution, dissipative terms are added to the equations. Jameson (ref. 6), via numerical experiments, developed a blend of second and fourth difference smoothing operators. The operator $D(\underline{u})$ in equation (6) can be decomposed into three spatial operators

$$D(\underline{u}) = (D_r + D_\theta + D_z)(\underline{u})$$

such that the dissipation in each direction can be evaluated separately. The dissipation in the axial direction, $D_z(\underline{u})$, is expressed as follows

$$D_z(\underline{u}) = d_{i+1/2,j,k} - d_{i-1/2,j,k} \quad (7)$$

where

$$d_{i+1/2,j,k} = \frac{Vol_{i+1/2,j,k}}{\Delta t_{i+1/2,j,k}} \left[\varepsilon^2_{i+1/2,j,k} \, \Delta_z \, \underline{u}_{i,j,k} - \varepsilon^4_{i+1/2,j,k} \, \Delta_a^3 \underline{u}_{i,j,k} \right] \tag{8}$$

and the coefficients ε^2 and ε^4 are evaluated as follows:

$$\varepsilon^2_{i+1/2,j,k} = \kappa^2 \max(\nu_{i+1,j,k}, \nu_{i,j,k})$$

$$\varepsilon^4_{i+1/2,j,k} = \max\left(0, \kappa^4_{i+1/2,j,k} - \varepsilon^2_{i+1/2,j,k}\right)$$

κ^2 and κ^4 are constants typically set at 1/2 and 1/64, respectively. To capture shocks sharply and retain second-order accuracy away from shocks, Jameson defined the coefficient $\nu_{i,j,k}$ as

$$\nu_{i,j,k} = \text{abs}\left[\frac{P_{i+1,j,k} - 2P_{i,j,k} + P_{i-1,j,k}}{P_{i+1,j,k} + 2P_{i,j,k} + P_{i-1,j,k}}\right] \tag{9}$$

The variable $\nu_{i,j,k}$ is proportional to the square of the mesh spacing in smooth regions of flow and linear in mesh spacing in regions of large pressure gradients. The pressure sensitive switch was applied only in the axial and circumferential directions. For the radial direction, it was found that setting $\nu_{i,j,k}$ to a constant (0.05) and ε^4 to zero enhanced the stability of the scheme.

Boundary Conditions

The mathematical form of the field equations solved in the present work closely resembles that of the Euler equations. Therefore, the known mathematical properties of the Euler equations will be used as a guide to develop the boundary conditions of the present system of equations. It is assumed that the absolute flow field approaching and leaving the propeller is subsonic. This implies that four conditions must be specified at the upstream boundary and only one at the downstream boundary.

The axial velocity component and the flow properties at the upstream boundary are updated based on a local unsteady one-dimensional flow model in which the entropy is assumed constant with time and uniform in space. The equations associated with this model are

$$\frac{dC^-}{dt} + (v_z - a)\frac{\partial C^-}{\partial z} = 0 \tag{10a}$$

$$\frac{dC^+}{dt} + (v_z - a)\frac{\partial C^+}{\partial z} = 0 \tag{10b}$$

In which C^+ and C^- are the well-known Riemann invariants. They are related to the axial velocity, v_z, and speed of sound, a, by the equations:

$$v_z + \frac{2a}{\gamma - 1} = C^+, \quad v_z - \frac{2a}{\gamma - 1} = C^-$$

The invariant C^+ is associated with information coming from outside the computational domain and thus it is specified based on the far field flow conditions. The C^- invariant is updated by solving equation (10b) in time using the Runge-Kutta integration procedure outlined earlier. The axial derivative is approximated by a backward difference operator. The Riemann invariants determine the speed of sound and the axial velocity component. The pressure, density, and temperature are updated based on the known value of the incoming entropy. The value of the velocity components parallel to the upstream boundary are assumed known.

At the downstream boundary, simple radial equilibrium is enforced.

$$\frac{\partial p}{\partial r} = \frac{\rho v_r^2}{r} \tag{11}$$

The pressure is specified at the free-stream farfield boundary and equation (11) is integrated radially using the trapezoidal rule toward the spinner-nacelle. The remaining flow variables are extrapolated from the interior.

Boundary conditions at the farfield boundary are derived based on a one-dimensional unsteady flow model identical to the one employed at the upstream boundary. In this model, the axial velocity component is replaced by the radial component. The value of C^+ is fixed by the farfield condition and C^- is extrapolated from the interior.

At periodic flow boundaries we require the flow to exhibit a spatial periodicity equal to the pitch of the blade row. Thus, any information required from a cell which lies adjacent to a periodic boundary but outside the computational domain is obtained from a cell which also lies adjacent to a periodic boundary but is inside the computational domain.

Since the flux is zero on solid surfaces only the pressure need be known. This can be extrapolated from the interior or determined from an adaptation to the present system of equations of a normal pressure gradient condition developed by Rizzi (ref. 6). The present work uses the adapted Rizzi condition on the hub and extrapolation for the blade surfaces.

Mesh Generation

To solve the average-passage equation system through a multiblade row machine, a mesh is needed for each blade row which contains the axial and radial coordinates of all blade rows. Thus, for a two-stage machine, four grids would be generated and each assigned the thickness and period of one of the four blade rows. However, each mesh must also conform axisymmetrically to the coordinates of the other blade rows. To do this efficiently, the geometry is separated into blade and nonblade sections from inlet to exit. An

axisymmetric algebraic mesh is generated using two-dimensional spline fits and the axial and radial coordinates are common to all the grids in the meridional plane. To complete the grids, the tangential mesh lines are generated using spline fits and taking into account blade thickness and blade count.

Solution Procedure

A nested iteration procedure using an inner and outer loop was presented in reference 9 to solve the average-passage equation system through each blade row of a multiblade row machine. Within the inner loop the three-dimensional "average" flow variables are evaluated for a given distribution of body forces, energy sources, and correlations. These terms are denoted as $\underline{S}$ in equation (5). The inner loop uses the Runge-Kutta integration procedure outlined earlier for solving the Euler-like equations. The outer loop updates the body forces, energy sources, and correlations based on the axisymmetric average of the converged inner loop solution. An outline for updating the above terms can be found in reference 9. Global or outer loop convergence is obtained when the differences between the axisymmetric average of the time-average flow variables on each blade row is below a given tolerance.

RESULTS AND DISCUSSION

A General Electric counter-rotating unducted fan configuration was simulated on a Cray 1-S. The geometry contains two, eight-bladed fans (fig. 2) designed to operate at a free-stream Mach number of 0.72 and advance ratio of 2.80. The grid (fig. 3) contains 99 axial, 36 radial, and 16 circumferential points with 28 points lying forward of the front blade, 20 points axially on both blades, 15 points between blades, and 15 points aft of the rear blade. Both blades contain 22 equally spaced points in the radial direction with the remaining 14 spaced from the blade tip to the free-stream. No mesh clustering was used in the angular direction. A sting whose diameter was equal to the sting at the hub exit was affixed to the front of the nacelle.

Figures 4 and 5 show contours of constant relative Mach number on the pressure and suction side of the forward and aft blade rows. The shock location on the suction side of both blades (figs. 4(a) and 5(a)) run along the trailing edge of the blade terminating at about 30 percent of span on the first propeller. One would expect to observe this shock structure given the high inlet Mach number and blade geometry. There also appears to be a shock in the vicinity of the nacelle/suction surface interface for the forward propeller. Figure 5(b) shows the presence of a supersonic bubble at the junction of the nacelle surface on the pressure side of the aft blade. This bubble seems to extend across the passage to the suction surface indicating that the flow in the hub region is choked.

The forward blade was also run in isolation using the same spinner-nacelle geometry. The inlet Mach number and rotational speed were identical to those for the counter-rotating configuration. The relative Mach number contours are illustrated in figure 6 for the suction and pressure surfaces. Note that the Mach numbers in general are lower than those which appear on the forward propeller of the counter-rotating configuration. This is attributed to the "induction" effect of the second blade row. More fluid passes through the counter-rotating configuration than through the isolated configuration. This

can be seen more readily in plots of relative Mach number versus axial distance. Three radial stations are shown in figures 7 to 9. It is seen that the relative Mach number forward and aft of the first blade row is higher for the counter-rotating configuration than it is for the isolated configuration. The shock strength for both configurations appear to be the same, however, for the counter-rotating configuration the shock location is nearer the blade trailing edge.

There are a number of ways to determine convergence of the above simulations. Jameson typically computes the time derivative of the density (i.e., $\partial\rho/\partial t$), and the number of supersonic points. Figures 10 show plots of $\partial\rho/\partial t$ versus the number of cycles for the first and second blade row simulation. The solid line indicates the maximum absolute value of the derivative and the dashed line the average value of the derivative. The average value is determined by evaluating the sum of the absolute value of the time derivative at each point in the field divided by the number of points. The peaks at every 500 cycles are attributed to updating the body forces, energy sources, and correlations. It is seen that the present solution strategy for solving the inner loop equations converges as indicated by the reduction in both the maximum and average levels of $\partial\rho/\partial t$. Figure 11 show the number of supersonic points based on the absolute Mach number versus the number of calculation cycles. Again, the number of supersonic points for both simulations converges to a constant value further indicating convergence. Finally, figure 12 measures the L_2 norm of the difference of the axisymmetrically-averaged solutions calculated at the end of each outer loop. The L_2 norm shows a drop of two orders of magnitude. This reduction was judged sufficient to consider the computations converged.

As a final check on the solutions described above, they were compared to experimental measurement taken in the NASA Lewis 8 by 6 Tunnel (ref. 10). This comparison is shown in figure 13. The solid and dashed line is a plot of the axisymmetrically-averaged static pressure along the nacelle obtained from the first and second blade row simulations, respectively. The diamonds represent the experimental data. There is good agreement between the prediction and measurement aft of the maximum nacelle diameter. The discrepancy at the spinner-nacelle nose was expected since the physical domain did not conform to the true nacelle geometry in this region. The grid conformed to a sting having the same diameter as the sting attachment at the end of the model.

Since the above computations required large memory and CPU time, some code enhancements are being pursued. These include multitasking and minimization of in-core storage. The first attempt at multitasking required the resources of a Cray X-MP multiprocessor computer. This effort involved assigning the flow field simulation associated with each blade row to a processor. This step alone decreased run time by a factor of two for a two blade row configuration. Also, due to the advanced architecture of the Cray X-MP compared to the Cray 1-S, an additional speedup was obtained. The net result was a reduction in CPU time by a factor of three over a comparable simulation on the Cray 1-S. To minimize in-core storage, the three-dimensional solutions will be stored in two-dimensional planes on secondary storage. To minimize I/O overhead, the use of a high speed mass storage device will be needed. By implementing these two enhancements, the capabilities of the code can be extended to solve multistage problems.

CONCLUSIONS

A numerical procedure based on a finite volume formulation was developed to solve the average-passage equation system for a multiblade row configuration. This procedure employed a four-stage Runge-Kutta integration scheme to march the equations forward in time towards the time asymptotic limit. A computer code based on this procedure was successfully used to simulate the average-passage flow fields associated with a high speed counter-rotating propeller. The results of this simulation yielded information which proved useful in evaluating aerodynamic design.

ACKNOWLEDGMENTS

The authors would like to express their thanks to Mr. Tom Sullivan of GE Evandale and Dr. Larry Bober and Mr. Bob Jeracki of NASA Lewis for their helpful comments, suggestions, and assistance in developing the results pertaining to these computations.

REFERENCES

1. Adamczyk, J.J., "Model Equation for Simulating Flows in Multistage Turbomachinery," NASA TM-86869 and ASME 85-GT-226, November 1984.

2. Bober, L.J., Chaussee, D.S. and Kutler, P., "Prediction of High-Speed Propeller Flow Fields Using a Three-Dimensional Euler Analysis," NASA TM-83065 and AIAA-83-0188, January, 1983.

3. Barton, J.M., Yamamoto, O., and Bober, L.J., "Inviscid Analysis of Advanced Turboprop Propeller Flow Fields," AIAA-85-1263, July, 1985.

4. Clark, B.J. and Scott, J.R., "Coupled Aerodynamic and Acoustical Prediction for Turboprops," 107th Meeting of the Acoustical Society of America, Norfolk, VA, May 7-10, 1984.

5. Holmes, D.G. and Tong, S.S., "A Three-Dimensional Euler Solver for Turbomachinery Blade Rows," ASME 84-GT-79, June 1984.

6. Jameson, A., Schmidt, W., and Turkel, E., "Numerical Solutions of the Euler Equations by Finite Volume Methods Using Runge-Kutta Time-Stepping Schemes," AIAA-81-1259, June 1981.

7. Celestina, M.L. and Adamczyk, J.J., "Three-Dimensional Euler Solver for Turbomachinery," presented at NASA Marshall SSME CFD Workshop, Huntsville, Alabama, November 1984.

8. Denton, J.D. and Singh, U.K., "Time Marching Methods for Turbomachinery Flow Calculations," VKI Lecture Series 1979-7, Rhodes Saint Genese Belgium, April 1979.

9. Adamczyk, J.J., Mulac, R.A., and Celestina, M.L., "A Model for Closing the Inviscid Form of the Average-Passage Equation System," Submitted for presentation at the 1986 ASME International Gas Turbine Conference.

10. Jeracki, B., Private communications.

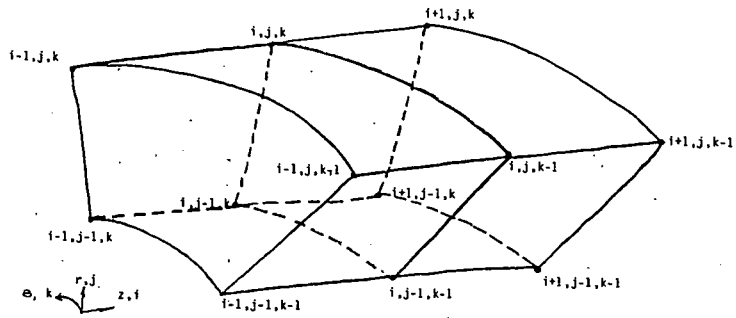

Figure 1. - Typical cell in cylindrical coordinate system.

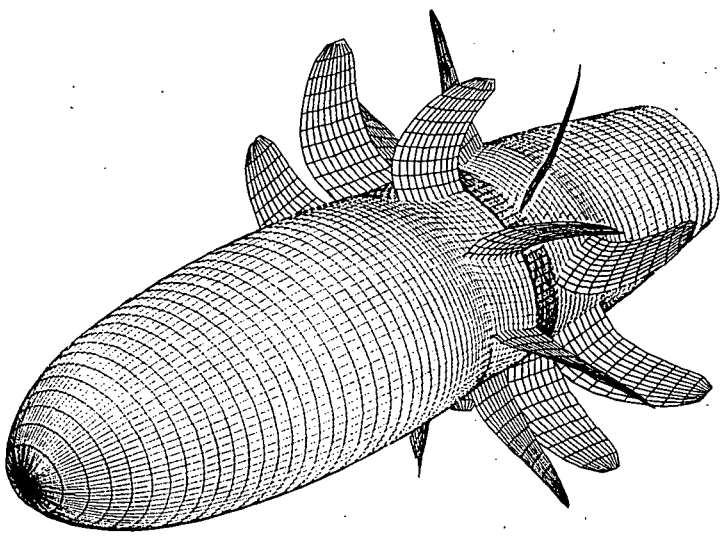

Figure 2. - General Electric unducted fan configuration.

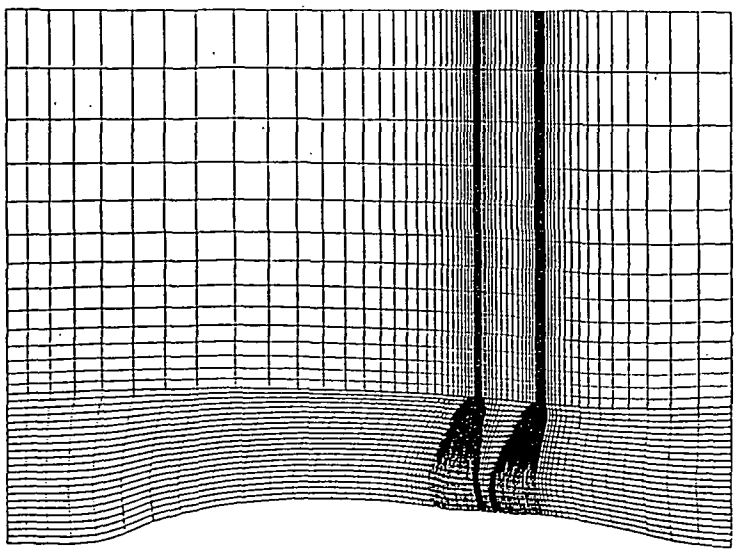

(a) Constant ζ cut for forward and aft propellers.

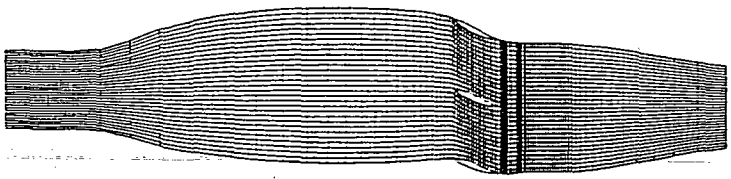

(b) Constant η cut for forward propeller.

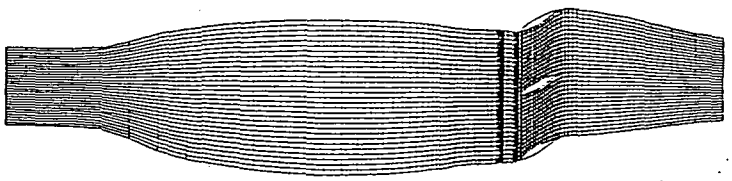

(c) Constant η cut for aft propeller.

Figure 3. - GE unducted fan grid (99x36x16).

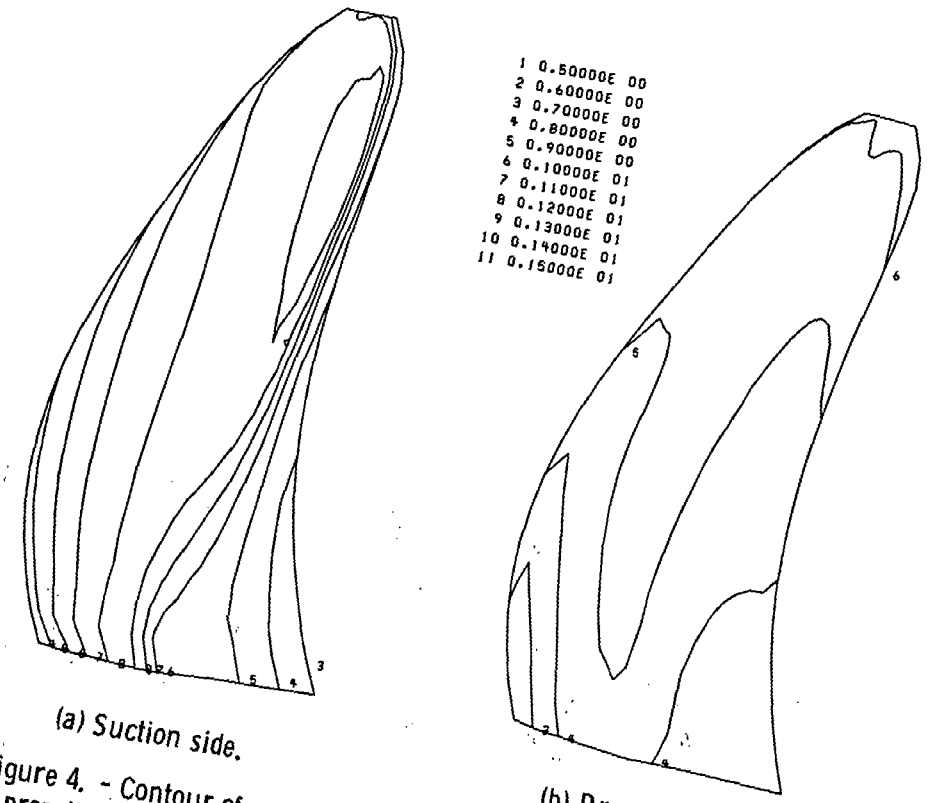

(a) Suction side.

(b) Pressure side.

Figure 4. - Contour of constant relative Mach number for forward propeller. $M_\infty = .72$, $J = 2.80$.

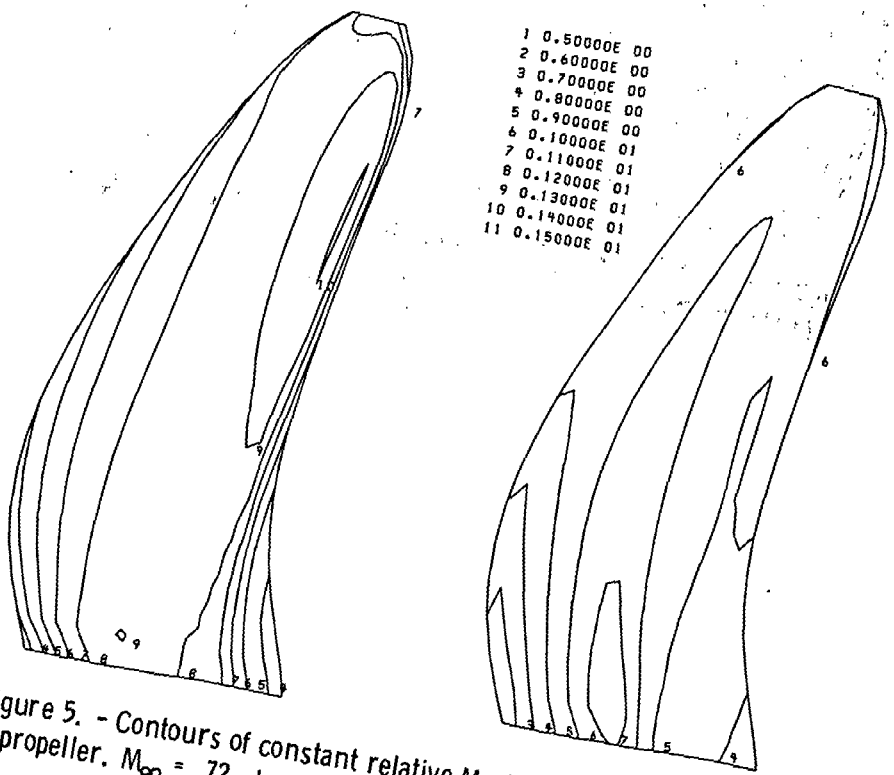

Figure 5. - Contours of constant relative Mach number for aft propeller. $M_\infty = .72$, $J = -2.80$.

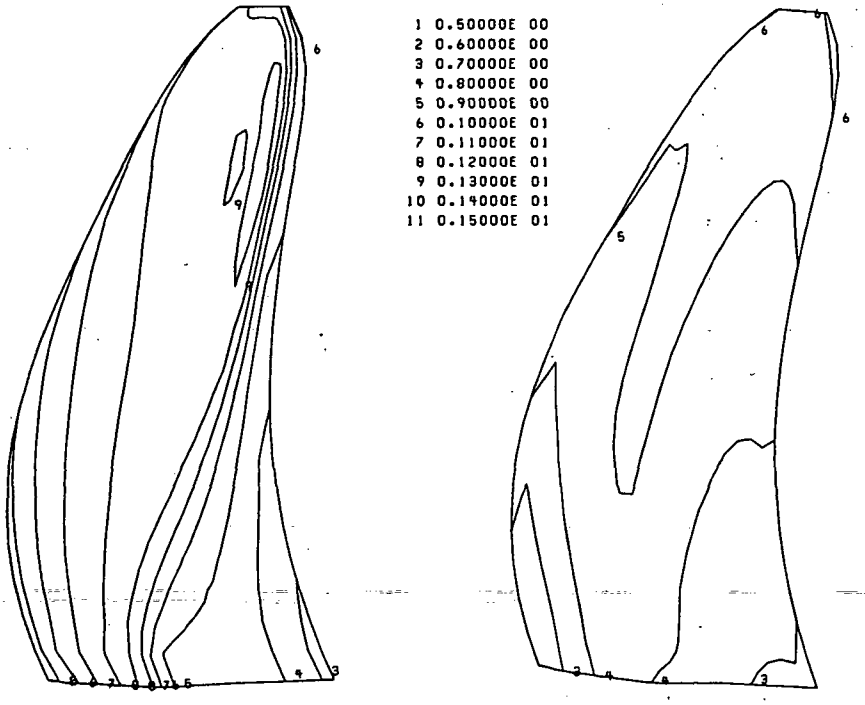

Figure 6. - Contours of constant relative Mach number for forward propeller in isolation. $M_\infty = .72$, $J = 2.80$.

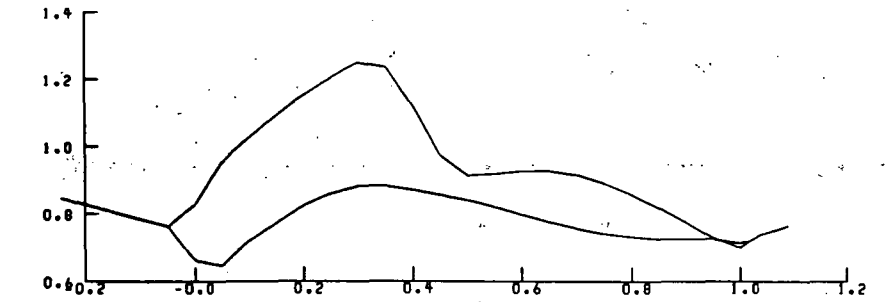

(a) 10% span.

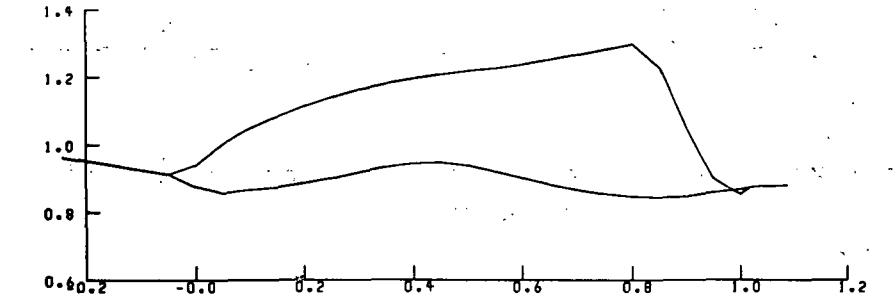

(b) 50% span.

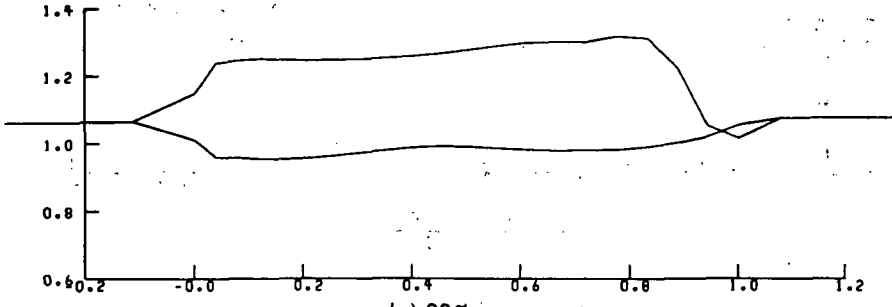

(c) 90% span.

Figure 7. - Relative Mach number vs axial distance on blade surface. Forward propeller.

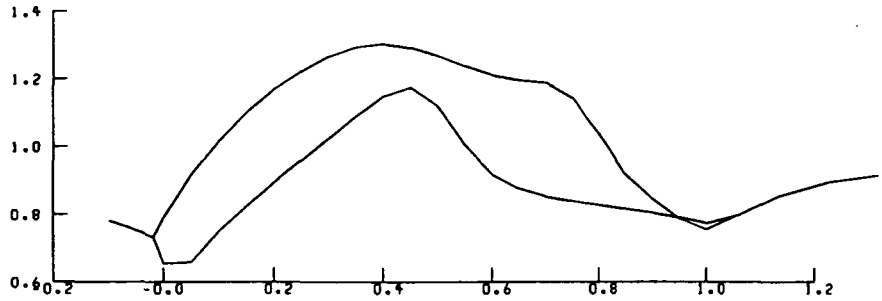

(a) 10% span.

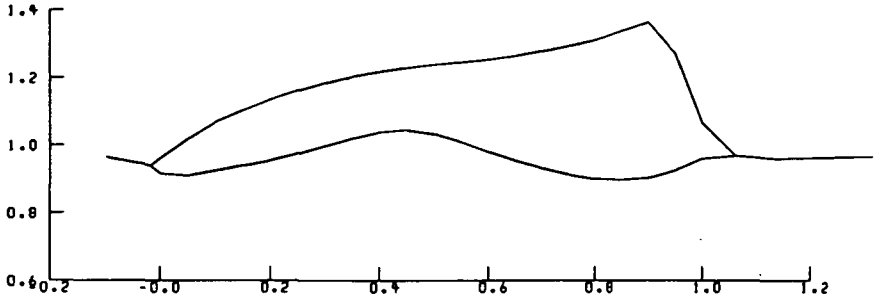

(b) 50% span.

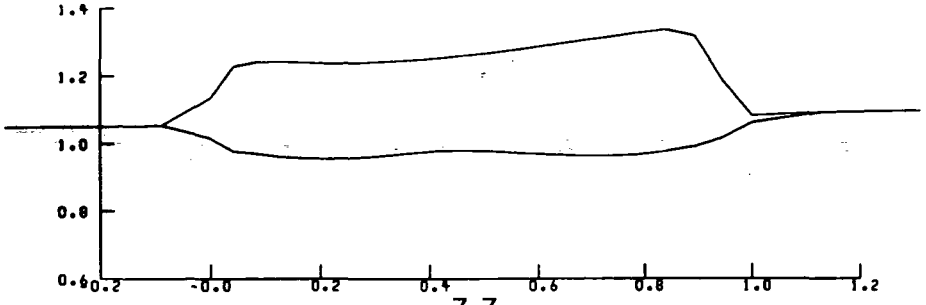

$$\frac{Z-Z_{LE}}{Z_{TE}-Z_{LE}}$$

(c) 90% span.

Figure 8. - Relative Mach number vs axial distance on blade surface. Aft propeller.

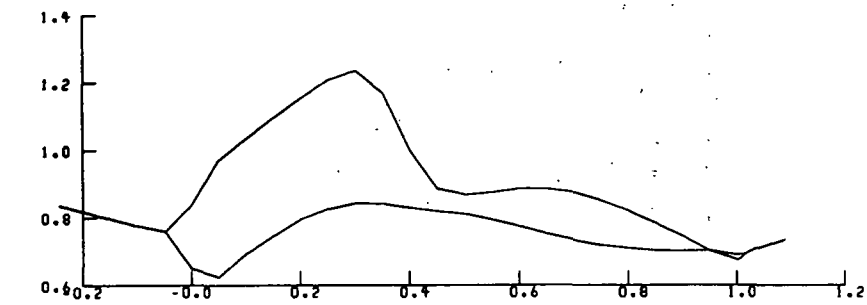

(a) 10% span.

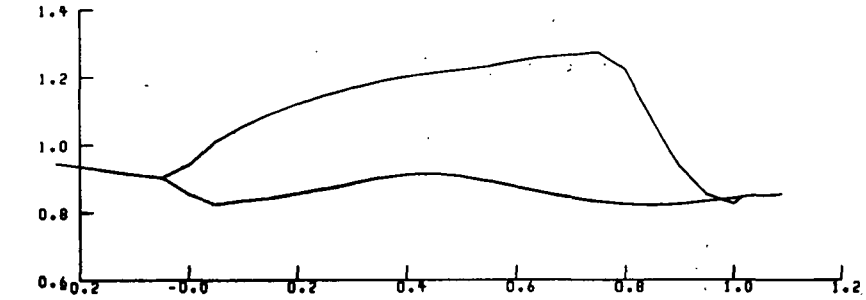

(b) 50% span.

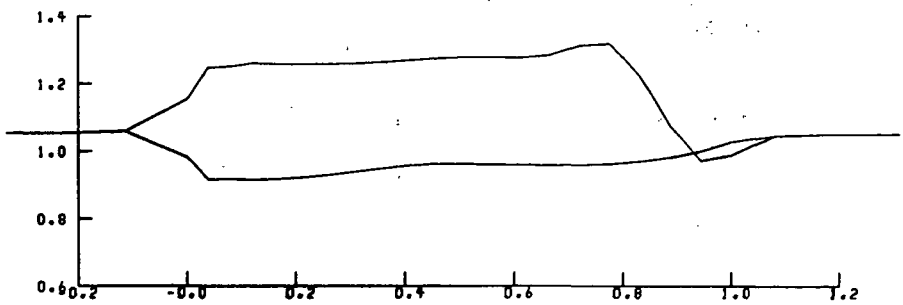

(c) 90% span.

Figure 9. - Relative Mach number vs axial distance on blade surface. Forward propeller in isolation.

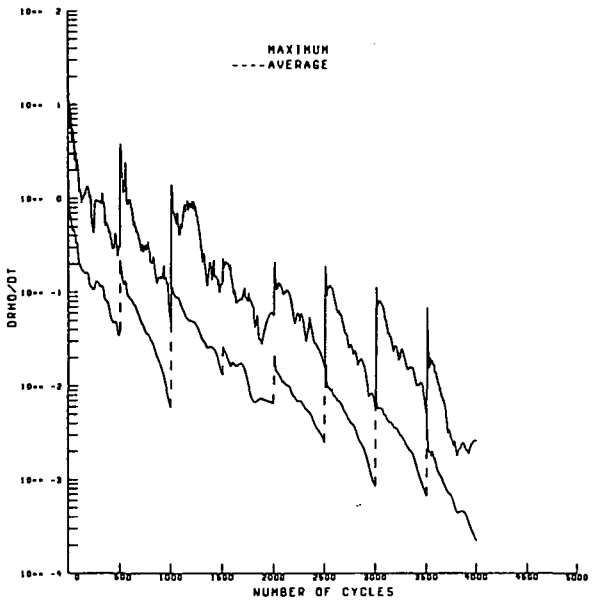

(a) Forward propeller solution.

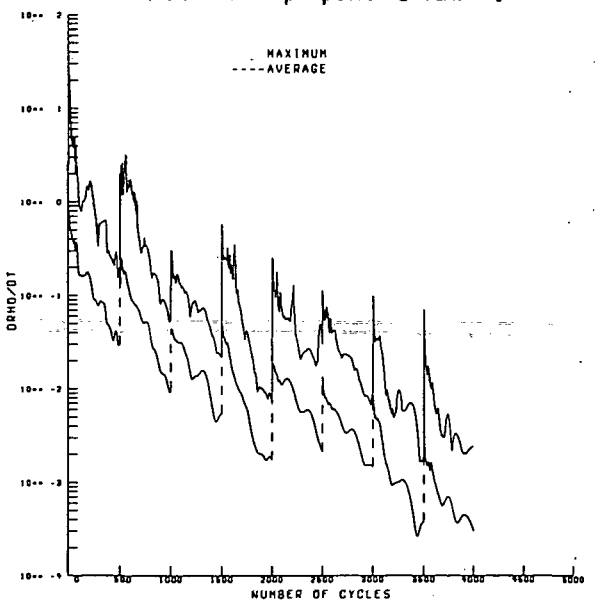

(b) Aft propeller solution.

Figure 10- Convergence history for forward and aft propeller.

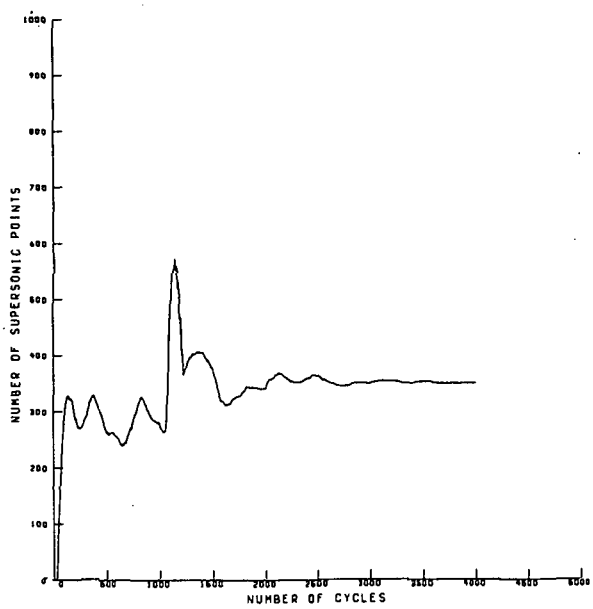

(a) Forward propeller solution.

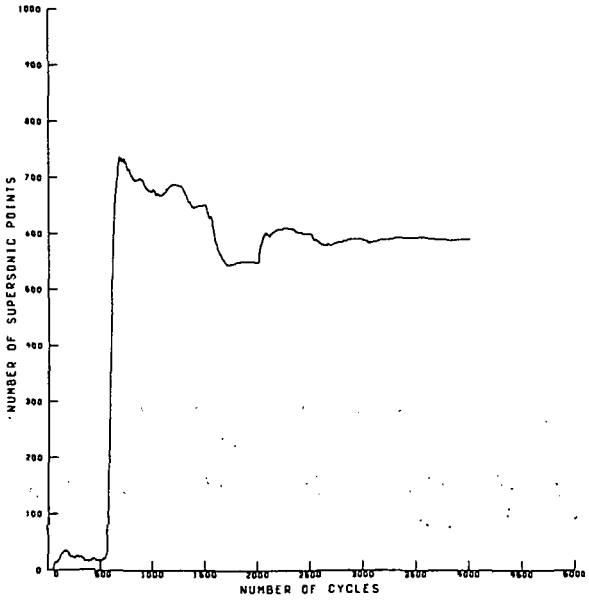

(b) Aft propeller solution.

Figure 11. - Convergence based on number of supersonic points.

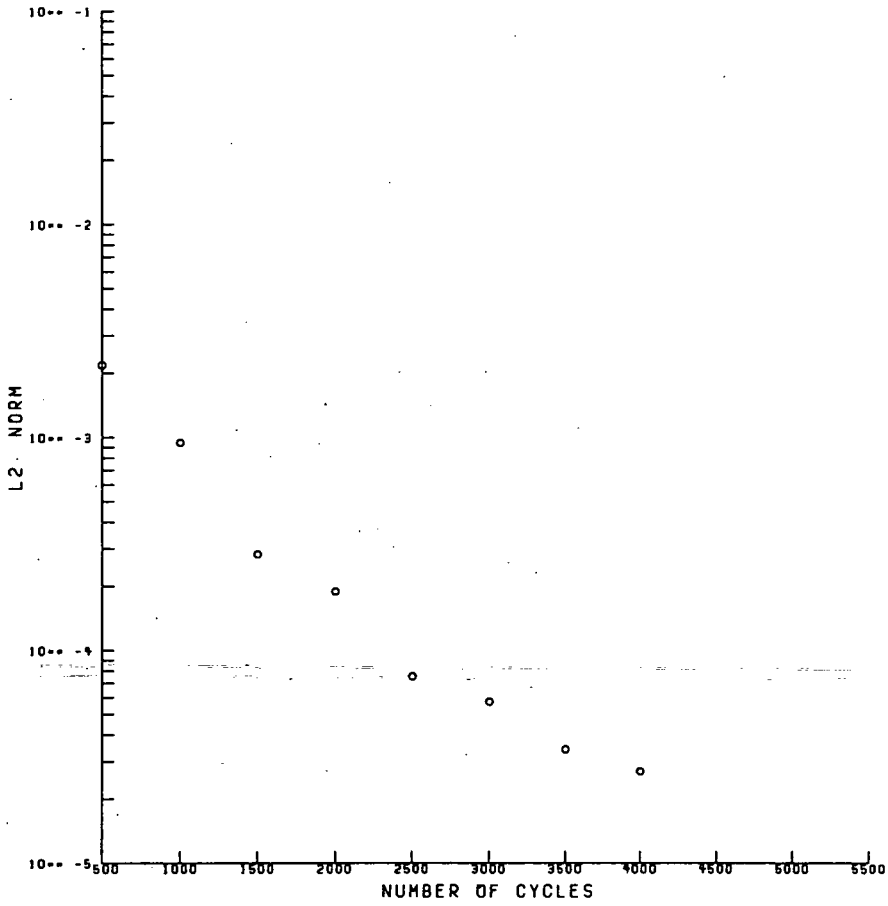

Figure 12. - L_2 norm of difference between axisymmetrically-averaged solutions.

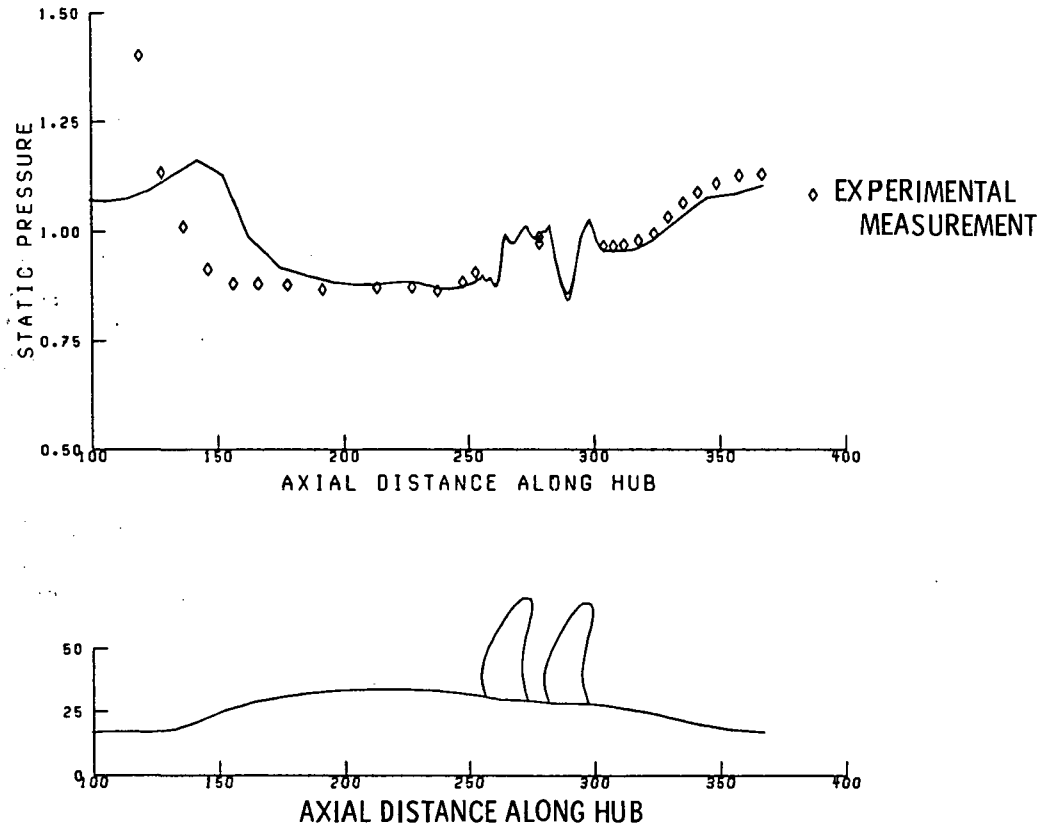

Figure 13. - Spinner Nacelle axisymmetric static pressure distribution.

1. Report No.	2. Government Accession No.	3. Recipient's Catalog No.
NASA TM-87200		

4. Title and Subtitle	5. Report Date
A Numerical Simulation of the Inviscid Flow Through A Counter-Rotating Propeller	6. Performing Organization Code: 505-90-01

7. Author(s)	8. Performing Organization Report No.
Mark L. Celestina, Richard A. Mulac, and John J. Adamczyk	E-2855
	10. Work Unit No.

9. Performing Organization Name and Address	11. Contract or Grant No.
National Aeronautics and Space Administration Lewis Research Center Cleveland, Ohio 44135	13. Type of Report and Period Covered: Technical Memorandum

12. Sponsoring Agency Name and Address	14. Sponsoring Agency Code
National Aeronautics and Space Administration Washington, D.C. 20546	

15. Supplementary Notes

Mark L. Celestina, Richard A. Mulac, Sverdrup Technology, Inc., Lewis Research Center, Cleveland, Ohio 44135; John J. Adamczyk, NASA Lewis Research Center. Prepared for the 31st International Gas Turbine Conference, sponsored by the American Society of Mechanical Engineers, Dusseldorf, West Germany, June 8-12, 1986.

16. Abstract

This paper presents the results of a numerical simulation of the time-averaged inviscid flow field through the blade rows of a multiblade row turboprop configuration. The governing equations are outlined along with a discussion of the solution procedure and coding strategy. Numerical results obtained from a simulation of the flow field through a modern high-speed turboprop will be shown.

17. Key Words (Suggested by Author(s))	18. Distribution Statement
Internal flow; Turbomachinery flow	Unclassified - unlimited STAR Category 02

19. Security Classif. (of this report)	20. Security Classif. (of this page)	21. No. of pages	22. Price*
Unclassified	Unclassified		

*For sale by the National Technical Information Service, Springfield, Virginia 22161

National Aeronautics and
Space Administration

Lewis Research Center
Cleveland, Ohio 44135

SECOND CLASS MAIL

ADDRESS CORRECTION REQUESTED

Postage and Fees Paid
National Aeronautics and
Space Administration
NASA-451

NASA